JCIM JOURNAL OF CHEMICAL INFORMATION AND MODELING

pubs.acs.org/jcim Article

Dissecting Reaction Mechanisms and Catalytic Contributions in Flavoprotein Fumarate Reductases

Felipe Curtolo and Guilherme M. Arantes*

Cite This: https://doi.org/10.1021/acs.jcim.3c00292 Read Online

ACCESS | Metrics & More | Article Recommendations | Supporting Information

ABSTRACT: The interconversion between fumarate and succinate is fundamental to the energy metabolism of nearly all organisms. This redox reaction is catalyzed by a large family of enzymes, fumarate reductases and succinate dehydrogenases, using hydride and proton transfers from a flavin cofactor and a conserved Arg side-chain. These flavoenzymes also have substantial biomedical and biotechnological importance. Therefore, a detailed understanding of their catalytic mechanisms is valuable. Here, calibrated electronic structure calculations in a cluster model of the active site of the Fcc_3 fumarate reductase were employed to investigate various reaction pathways and possible intermediates in the enzymatic environment and to dissect interactions that contribute to catalysis of fumarate reduction. Carbanion, covalent adduct, carbocation, and radical intermediates were examined. Significantly lower barriers were obtained for mechanisms via carbanion intermediates, with similar activation energies for hydride and proton transfers. Interestingly, the carbanion bound to the active site is best described as an enolate. Hydride transfer is stabilized by a preorganized charge dipole in the active site and by the restriction of the C1−C2 bond in a twisted conformation of the otherwise planar fumarate dianion. But, protonation of a fumarate carboxylate and quantum tunneling effects are not critical for catalysis of the hydride transfer. Calculations also suggest that the driving force for enzyme turnover is provided by regeneration of the catalytic Arg, either coupled with flavin reduction and decomposition of a proposed transient state or directly from the solvent. The detailed mechanistic description of enzymatic reduction of fumarate provided here clarifies previous contradictory views and provides new insights into catalysis by essential flavoenzyme reductases and dehydrogenases.

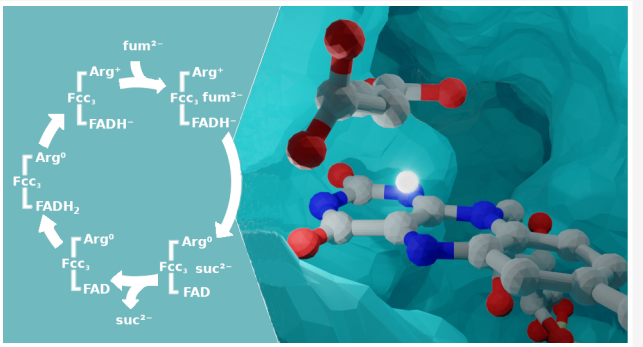

INTRODUCTION

Fumarate reductases (FRD) and succinate dehydrogenases (SDH) are homologous flavoenzymes that catalyze the interconversion between fumarate and succinate in anaerobic and aerobic respiration, respectively.[1] They are essential for energy metabolism and cell homeostasis, and at least one orthologous gene is found in all aerobic and most anaerobic organisms.[2,3] Inhibition of FRD/SDH enzymes can potentially be used to treat cancer and parasitic infections[4] or to avoid ischemia-reperfusion injury.[5] These enzymes also have biotechnological relevance as ene-reductases for stereoselective hydrogenations.[6]

While their origin can be traced to a single soluble protein ancestor,[7,8] membrane-bound FRD/SDH enzymes found in prokaryotes and in the inner mitochondrial membrane have evolved to multimeric complexes with iron−sulfur proteins and transmembrane subunits.[1] Soluble FRDs are monomeric and found in bacterial periplasm[9] and various cellular compartments.[10] They are easier to manipulate; hence, experimental studies often employ the soluble FRD flavocytochrome c_3 (Fcc_3) of *Shewanella frigidimarina*.[6,11−18] A large part of our understanding of succinate oxidation in respiratory complex II also stems from investigations in Fcc_3.[1]

The FRD/SDH active site is held by highly conserved clamp and FAD-binding domains.[3,11,19,20] Upon binding, the substrate (fumarate or succinate) stacks between the isoalloxazine ring of a flavin adenine dinucleotide (FAD) and the guanidinium side-chain of a catalytic Arg in the active site[11,13,21] (Scheme 1). Additional His, Thr, and Arg side-chains also contribute to substrate orientation and polarization (Figure 1a).[14,22,23] This active site topology is highly conserved and suggests ubiquitous reaction mechanisms.[1,11] Remarkably, membrane-bound FRD/SDHs have evolved to covalently attach the flavin ring to a His side-chain, facilitating succinate oxidation.[8,24]

Received: February 24, 2023

Scheme 1. Fumarate Reduction to Succinate Catalyzed by the Flavin Ring (FAD) and Arg Side-Chain (R402 in Fcc_3 Numbering) in FRD/SDH Enzymes

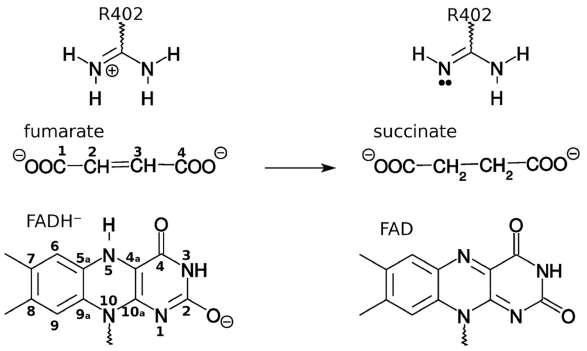

Fumarate reduction proceeds through addition of two protons and two electrons to the C2═C3 double bond (Scheme 1). A hydride equivalent is transferred from $FADH^-$ (most probably nitrogen N5) to fumarate (carbon C2),[6,11] with the other proton coming from the catalytic Arg[14,15,25] (Arg402 in Fcc_3 *S. frigidimarina* numbering used hereafter). A Grotthuss-like pathway involving conserved residues (Glu378) has been proposed to allow fast proton transfer from the solvent to regenerate protonated Arg402.[14,18] To reduce FAD, electrons are provided by the attached iron−sulfur protein in most FRD/SDH enzymes or from a chain of heme groups in Fcc_3.[11]

However, mechanistic details and the sequence of hydride and proton transfers to fumarate are not clearly understood.[26] Kinetic isotope effects suggest disputable views between concerted and stepwise mechanisms.[27−29] Observation of an "intermediate-like" molecule in the active site of some crystallographic structures was interpreted as evidence of a stepwise mechanism.[11,30] Thus, it is mostly accepted that fumarate reduction proceeds in two distinct steps with hydride transfer from $FADH^-$ first generating a carbanion as reaction intermediate.[1,16,22] This stepwise mechanism was probed in a computational study[31] with a minimal model of the active site, suggesting that hydride transfer is rate-limiting and that the enzyme employs a relay acid catalysis with His504 protonating carboxylate C4 of fumarate prior to hydride transfer.

We have previously shown in an isolated model reaction that addition of a hydride equivalent from $FADH^-$ to fumarate may not proceed as a prototypical hydride transfer but with proton and electrons moving asynchronously and to different parts of the molecule.[26] Moreover, alternative reaction mechanisms may be employed in the FRD/SDH active site. For instance, when a carbanion intermediate is formed, its electron density can be shared with FAD and form a covalent adduct, as observed in similar flavin reactions.[32] Proton transfer from Arg402 to fumarate C═C before complete reduction could also be possible. Instead of a classical carbocation, a radical intermediate with an accompanying electron from $FADH^-$ may be generated, in a proton-coupled electron transfer (PCET).[26] Proton transfer might also occur concerted to the nucleophilic attack of $FADH^-$ toward fumarate and lead to another covalent adduct, as observed in a hydratase flavoenzyme.[33]

Various catalytic effects have been proposed to accelerate fumarate reduction in FRD/SDH enzymes.[1,11] Geometric distortion of bound fumarate by twisting the C1−C2 bond (Scheme 1) has been suggested to destabilize the substrate[20] and prevent electron conjugation between the carboxylate group and the double bond, making the latter more prone to hydride addition.[11,21,23] Substrate polarization[1] and hydride quantum tunneling as shown in other flavoenzymes[34,35] may also contribute to catalysis in FRD/SDH.

The redox chemistry in the fumarate to succinate conversion is considered the rate-limiting step in the catalytic cycle of FRD/SDH.[12,36] Substrate binding and product unbinding are not kinetically relevant for enzyme turnover,[12,36] and enzyme regeneration is also considered to be fast, both FAD reduction and Arg402 reprotonation.[36,37] However, the sequence of product unbinding and FAD regeneration is questionable, with cyclic voltammetry indicating that FAD is regenerated in the

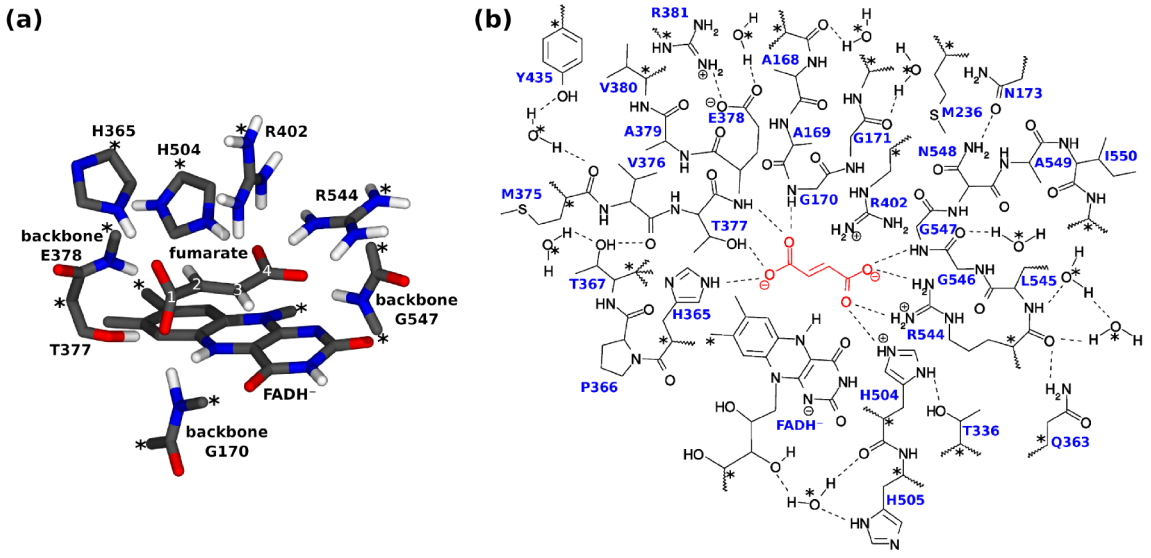

Figure 1. Models of the Fcc_3 active site from *S. frigidimarina* employed here. (a) Structure of the small cluster model. Only polar and fumarate hydrogens are shown. (b) Planar structural model of the large cluster with fumarate in red. Atoms labeled with * were kept frozen to maintain the active-site architecture.

https://doi.org/10.1021/acs.jcim.3c00292
J. Chem. Inf. Model. XXXX, XXX, XXX−XXX

unbound enzyme[36] and EPR experiments suggesting that FAD regeneration occurs when the product is still bound.[37]

Here, calibrated electronic structure calculations on a large cluster model of the Fcc_3 active site are employed to scrutinize the reaction mechanisms and find the most likely enzymatic pathway for reduction of fumarate. Then, proposed sources for the catalytic power in FRDs are dissected, particularly hydride tunneling, fumarate bond twisting, and electrostatic preorganization of the active site. Finally, a complete enzymatic cycle for Fcc_3 turnover is proposed based on the energetics of individual steps and in excellent agreement with the experimental redox potential of fumarate.

METHODS

Construction of the Active-Site Model. Small and large cluster models of the FRD active site were built based on the crystal structure with 1.8 Å resolution of Fcc_3 from *S. frigidimarina* bound to a malate-like intermediate.[11] The small cluster consisted of fumarate, anionic flavoquinol $FADH^-$, the catalytic Arg402, and the first shell of residues around fumarate. These are the side-chains of His365, Thr377, His504, and Arg544 and the backbones of Gly170, Glu378, and Gly547. Residues and $FADH^-$ were truncated as shown in Figure 1a. The large cluster (Figure 1b) is an expansion of the small model with a second shell of all residues within 10 Å of fumarate, that is Ala168, Ala169, Gly171, Asn173, Met236, Thr336, Gln363, Pro366, Thr367, Met375, Val376, Ala379, Val380, Arg381, Tyr435, Leu545, Gly546, Asn548, Ala549, Ile550, and nine structural waters. To maintain the active site architecture, atoms labeled with an * in Figure 1 were kept frozen. The small cluster comprised 121 atoms and was used for calibration of the model chemistry as presented in the Supporting Information (SI). The large cluster comprised 475 atoms and was used to obtain the reaction profiles and analyze the catalytic contributions.[38] Fumarate coordinates were obtained from the malate intermediate in the crystal structure,[11] with the oxygen in position 2 replaced by a hydrogen, and a hydrogen added in carbon 3 in the trans configuration with respect to the double bond. Initial coordinates used for geometry optimizations for both cluster models correspond to the Fcc_3 crystal structure.[11] Active site relaxation with geometry optimizations has been shown to be sufficiently accurate for large cluster models as employed here.[39] In the optimized reactant state (**1**), the distance of the hydride (bound to flavin N5) to fumarate C2 and to C3 is respectively 2.53 and 2.86 Å, corroborating that hydride transfer should proceed to C2.

The charge states of ionizable groups directly involved in catalysis[1] were assigned after previous results of site-directed mutagenesis, kinetics, structural and electrochemical studies.[14,22,36] Fully reduced FAD is in the anionic form $FADH^-$ under physiological pH for both soluble[12] and membrane-bound[36] members of the FRD/SDH family. Based on our previous calculations,[40] N3 and N5 were protonated. His504 had a positive charge (Hsp) based on the pK_a of 7.4 assigned experimentally.[14] His365 was neutral because it can be mutated to serine without loss of FRD activity[22] and protonated at Nϵ as Nδ accepts a hydrogen bond from a nearby peptide bond.[14] Arginine residues were all modeled in their charged state because of their high pK_a.[41] Arg402, which participates in the acid catalysis, is reprotonated by a Grotthuss-like proton delivery pathway.[14,18] Glu378 is in anionic form to salt-bridge with Arg381 and Arg402.[18] Finally, Tyr435 and His505 in the second shell were modeled as neutral (with Nδ protonated in His505). Fumarate was fully deprotonated as a dianion. Both small and large models have zero net charge.

Model Chemistry and Exploration of Energy Surfaces. Results reported in the main text employ the large cluster and the ωB97X-D3[42,43] functional with the def2-TZVPP basis set[44] to model reaction energetics and catalytic properties, except when mentioned otherwise. This functional was chosen after extensive calibration and testing of reaction intermediates studied here in comparison to high-level multiconfigurational and coupled-cluster wave function methods, as presented in the SI. The estimated uncertainty in the free energies presented below is 4 $kcal \cdot mol^{-1}$. This is the sum of the maximum absolute error of 3.3 $kcal \cdot mol^{-1}$ found for ωB97X-D3/def2-TZVPP energies in comparison to coupled-cluster reference calculations (SI) and the uncertainty in Hessians used to compute ZPVE and thermal contributions.[45] Energetics of the biradical intermediate **9** (Figure 3b) was treated with the partially contracted NEVPT2/CBS level[46,47] (see the SI for more details).

All single-point calculations and geometry optimizations were performed with ORCA version 4.1.1,[48,49] with the environment beyond the cluster model treated as an implicit solvent with the Conductor-like Continuum Polarization Model (C-PCM)[50] and a dielectric constant $\varepsilon = 4.0$.[39,51]

Geometries were optimized with density functional theory (DFT) using the composite method PBEh-3c[42,52−54] and increased integration grids (keyword "Grid5" in ORCA). This method corrects for basis set superposition errors and dispersion interactions and provides accurate geometries at the cost of a GGA-DFT functional.[52] For the small cluster, default geometry convergence settings were employed, but looser convergence criteria (keyword "LooseOpt") had to be employed for the large cluster. All optimized geometries were checked by inspecting if hydrogen bonds in the second solvation shell were maintained. For the small cluster, transition states (TSs) were fully optimized and checked by intrinsic reaction coordinate analysis.[55] For the large model, approximate TSs were generated by constrained geometry optimizations based on coordinates of reactive atoms in the small cluster. Hessian matrix calculations necessary for full TS optimizations are prohibitive for models with this size. All optimized geometries are available online.[56]

Zero-point vibrational energies (ZPVEs) and thermal and entropic contributions were calculated using the quasi rigid-rotor-harmonic-oscillator (RRHO) approximation[57] in temperature $T = 298$ K with the semiempirical tight-binding method GFN2-xTB,[58] again due to the large cluster size. To overcome nonzero gradients and imaginary frequencies, the single-point Hessian formalism of Spicher and Grimme[45] using a biased potential was employed. For transition states, regular Hessian calculations had to be used as the biased potential was unable to restrain the broken bond geometry. These calculations were performed with the `XTB` program version 6.3.3.[59]

Electrostatics and Tunneling Calculations. Proton potential and vibrational wave functions were calculated for the small cluster model in a two-dimensional grid using the Fourier grid Hamiltonian method.[60−62] The transmission coefficient κ was calculated with Wigner's first order correction for ground state tunneling.[63−65] Electronic nonadiabatic effects due to possible excited state crossings were probed for first-

https://doi.org/10.1021/acs.jcim.3c00292
J. Chem. Inf. Model. XXXX, XXX, XXX−XXX

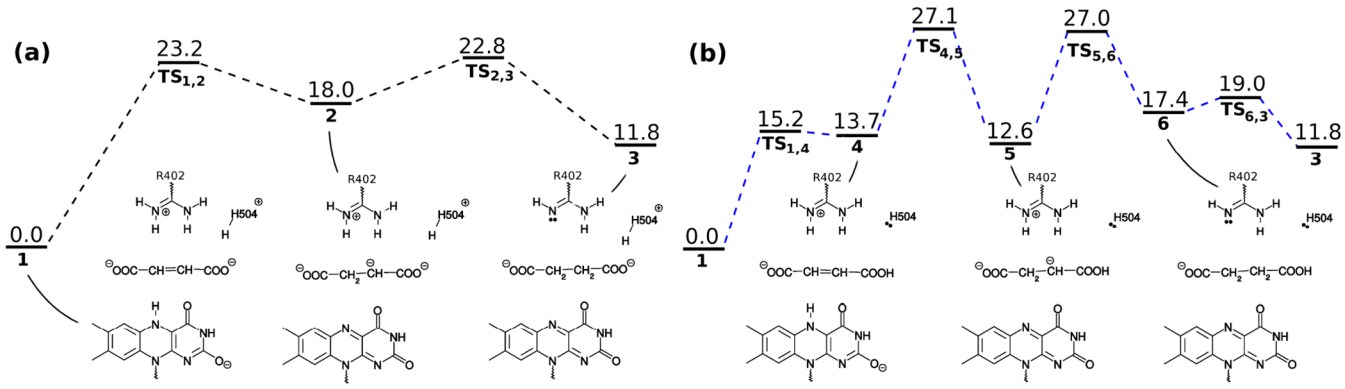

Figure 2. Free energy profiles (in kcal·mol^{-1}) for fumarate reduction via a carbanion intermediate with direct hydride transfer. In panel (a), fumarate carboxylates remain unprotonated, and in (b), fumarate C4 carbonyl is protonated by the cationic His504 side-chain. Free energies are shown over the profile bars, and species are identified by bold numbers placed below the bars. The model chemistry ωB97X-D3+C-PCM/def2-TZVPP//PBEh-3c with zero-point and thermal contributions at the GFN2-xTB level was employed.

excited singlets (S_1) with time-dependent DFT (TD-DFT) for species **1**, **2**, and $\mathbf{TS}_{1,2}$.

The electrostatic potential was calculated from the nuclear and electron density of the large cluster model with the `orca_vplot` program in ORCA[48,49] in a parallelepiped grid with 80 points in each dimension. The grid extended 3.5 Å beyond the cluster dimensions in order to map the electrostatics at molecular surfaces. All electrostatics and tunneling calculations employed the ωB97X-D3/def2-TZVPP level of theory.

RESULTS AND DISCUSSION

Fumarate Reduction Proceeds via a Carbanion/Enolate Intermediate. The large cluster model (Figure 1b) and a calibrated DFT model chemistry (SI Text) were used to investigate mechanisms of fumarate reduction by FADH$^-$ via carbanion, adduct, and radical intermediates. Reaction mechanisms show a proton transfer from Arg402 in a second step after the intermediate is formed, except for one reaction with an adduct intermediate (**1** → **8** below) and for the biradical intermediate (**9**).

Free energy profiles for nucleophilic addition via a carbanion intermediate with direct hydride transfer are shown in Figure 2. Without protonation of a fumarate carboxylate, hydride transfer from FADH$^-$ (**1** → **2**) has a barrier of 23.2 kcal·mol^{-1}, leading to a relatively unstable and, thus, transient intermediate **2**. Analysis of the electronic density for this species shows carbanion **2** is actually an enolate electromer (Figure 3 and the SI), so it will be referred to here as a carbanion/enolate, to keep consistency with previous studies.[1] During hydride transfer, electrons are transferred to molecular orbitals localized in fumarate C3, while the proton is asynchronously[66] added to fumarate C2, as we observed previously in an isolated flavin model reaction.[26]

Despite its high pK_a in water, Arg402 is easily deprotonated in the enzyme after intermediate **2** is formed, with a barrier of only 4.8 kcal·mol^{-1} for reaction **2** → **3**, showing the carbanion/enolate is a very strong base.

Because **1** is the rate-determining intermediate (TDI[67]), the effective activation energy of the reaction is 23 kcal·mol^{-1}, with both transition states $\mathbf{TS}_{1,2}$ and $\mathbf{TS}_{2,3}$ determining reaction kinetics. Note that these barriers are indistinguishable within the uncertainty of our calculations (see discussion in the SI). The interpretation that both steps contribute to reaction

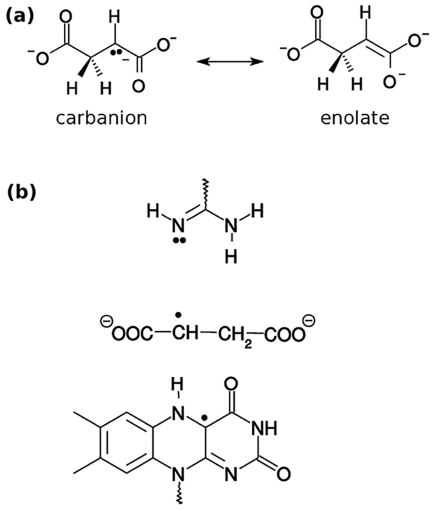

Figure 3. (a) Intermediate **2** (as well as **5** not shown here) formed after the hydride addition is actually an enolate electromer. (b) Biradical **9** formed after a multisite proton-coupled electron transfer.

kinetics agrees with experimental observations of slower enzyme turnover in D_2O[68] and contrasts to a previous computational work[31] that indicated hydride transfer was the only rate-limiting step.

Another reaction via a carbanion/enolate intermediate is possible with protonation of the fumarate C4 carboxylate by the cationic His504 side-chain (Figure 2b). The initial His504 proton transfer (**1** → **4**), hydride addition (**4** → **5**), and Arg402 proton transfer (**5** → **6**) have barriers of 15.2, 13.4, and 14.4 kcal·mol^{-1}, respectively. Despite these relatively low barriers, an effective activation energy of 27 kcal·mol^{-1} is found for this reaction (Figure 2b), corresponding to the free energy difference between the rate-determining transition states (TDTSs[67]) $\mathbf{TS}_{4,5}$ and $\mathbf{TS}_{5,6}$ and the rate-determining intermediate **1**.

Intermediate **5** is also described as an enolate electromer (Figure 3 and the SI). It is more stable than **2**; thus, protonation of fumarate by His504 stabilizes hydride addition. However, the initial proton transfer from cationic His504 has a high energetic cost (13.7 kcal·mol^{-1}), even though the neutral His504 formed in **4** can hydrogen-bond to Thr336 (with H504−Nδ) and to the protonated C4 carboxylate in fumarate

https://doi.org/10.1021/acs.jcim.3c00292
J. Chem. Inf. Model. XXXX, XXX, XXX−XXX

(with H504−Nϵ). Due to steric clashes and small conformational freedom for the substrate, it is unlike that a water molecule could fit in the active-site and hydrogen-bond to H504 or bridge the proton transfer to fumarate. Moreover, there is no evidence for such a water molecule in FRD/SDH experimental structures.[1,11]

Another possibility for direct addition mechanisms is the concerted hydride addition from $FADH^-$ with either proton transfer from Arg402 to form **3** in one single step or with proton transfer from His504 to form **5** followed by reprotonation of His504 from this intermediate concerted to proton transfer from Arg402. To be kinetically relevant, these highly concerted mechanisms would have to show activation energies lower than 23.2 kcal·mol^{-1}, as found for the stepwise direct addition **1** → **3**. Here, several attempts to find concerted TS were unsuccessful and resulted in stepwise $\mathbf{TS}_{1,2}$ or $\mathbf{TS}_{4,5}$, suggesting that any putative concerted TSs will have higher energies.

A second type of reaction intermediate was tested here, namely adducts with covalent bonds between fumarate and the flavin ring[32,33] (Figure 4). These adducts were proposed

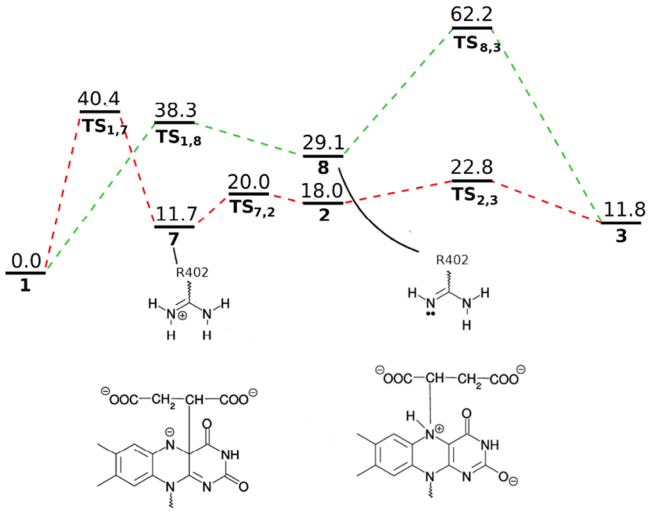

Figure 4. Free energies profiles (in kcal·mol^{-1}) for fumarate reduction with adduct formation and initial proton transfer from $FADH^-$ in red lines or from Arg402 in green lines.

because mass spectrometry studies suggested an adduct intermediate is formed in 2-haloacrylate hydratases, an enzyme from the FRD/SDH family.[33] Adducts can be formed in concert to hydride addition (**1** → **7**) or to proton transfer from Arg402 (**1** → **8**). Putative intermediate **7** can decompose to the carbanion/enolate **2** with reaction completion proceeding as in the direct hydride addition (Figure 2). Putative intermediate **8** can receive a hydrogen atom (HAT) and homolytically break the fumarate C2−N5 flavin bond to form the succinate product **3**. Free energy profiles (Figure 4) for these two adduct reactions show large barriers and should not be observed or play a role in the enzymatic mechanism. Alternative bond patterns, such as fumarate C3−N5 flavin, were not tested as they lead to longer hydride or proton transfer distances and, thus, should result in even higher barriers.

The third intermediate tested here was the biradical **9** (Figure 3). Instead of a classical carbocation, this biradical is formed spontaneously after a proton is transferred from Arg402 to fumarate-C3 in **1**, in a multisite[66] proton-coupled electron (from flavin ring) transfer. But, any mechanism passing through biradical **9**, or a higher energy classical carbocation, can be discarded due to its free energy of 60.0 kcal·mol^{-1} determined by multiconfigurational calculations [NEVPT2(6e,5o)+C-PCM/CBS//PBEh-3c, more details in the SI].

Therefore, direct hydride transfer without protonation (**1** → **2** → **3** profile in Figure 2a) is the most likely mechanism for enzymatic fumarate reduction in Fcc_3. Considering the uncertainty of 4 kcal·mol^{-1} suggested for our calculations (SI text), activation energies of 23 kcal·mol^{-1} and 27 kcal·mol^{-1} are hard to distinguish, and we cannot discard the participation of His504 as a relay general-acid catalyst (**1** → **5** → **3**). However, we can safely conclude that the reaction proceeds via nucleophilic addition by direct hydride transfer with a carbanion/enolate intermediate, as all the other adduct or radical (and carbocation) intermediates have significantly higher activation energies.

Hydride Transfer Has a Small Tunneling Contribution near the TS. After distinguishing between possible reaction mechanisms for fumarate reduction, it is clear that hydride transfer is a kinetically relevant step in the enzymatic reaction. Thus, it is important to investigate if tunneling effects contribute to the overall rate. We first note that reactions of $FADH^-$ with fumarate (**1** → **2** or **4** → **5**, Figure 2) are not prototypical hydride transfers but PCET reactions with the proton added to fumarate C2 and electrons delocalized over fumarate C3 and the adjacent carboxylate C4 to form the carbanion/enolate intermediate.[26] The adiabaticity regime of these reactions should be addressed before estimating the tunneling contribution.[69,70]

The small cluster model (Figure 1a) was employed here to probe the hydride transfer **1** → **2**. For fumarate **1**, $\mathbf{TS}_{1,2}$, and the carbanion/enolate intermediate **2**, the first singlet electronic excited state (S_1) is more energetic than the respective ground state (S_0) by 69.7, 72.5, and 64.0 kcal·mol^{-1}. Thus, electronic excited states are significantly more energetic and do not cross ground states along the hydride transfer (**1** → **2**) when thermally activated. This transfer is classified as electronically adiabatic,[71] and nuclei movement can be considered only in ground potential energy surfaces in the following treatment.

We assume tunneling may proceed near the $\mathbf{TS}_{1,2}$ and obtain vibrational wave functions only at this geometry. Figure 5b shows the two-dimensional proton potential generated by placing the transferring hydride in different positions along the plane formed by atoms N5 of $FADH^-$, C2 of fumarate, and the hydride position at the TS, with all other atoms held fixed in the $\mathbf{TS}_{1,2}$ geometry (Figure 5a). Minima at the reactant and product wells and the $\mathbf{TS}_{1,2}$ are labeled as star symbols. The energy difference $\Delta V_p^{\ddagger}$ between $\mathbf{TS}_{1,2}$ and the reactant minima in the proton potential is only 2.0 kcal·mol^{-1}, indicating an almost barrierless proton transfer potential, as is usually found in vibronically adiabatic PCET.[71]

Amplitudes of vibrational wave functions calculated for the transferring proton at this two-dimensional potential are shown in Figure 5c. In the ground vibrational state, the proton is delocalized between reactant and product wells, with the largest amplitudes around the TS geometry. For the first-excited vibrational state, the wave function has a larger amplitude around the reactant well. The energy splitting for the excited vibrational state Δ_{vib} = 2.7 kcal·mol^{-1} is higher than

https://doi.org/10.1021/acs.jcim.3c00292
J. Chem. Inf. Model. XXXX, XXX, XXX−XXX

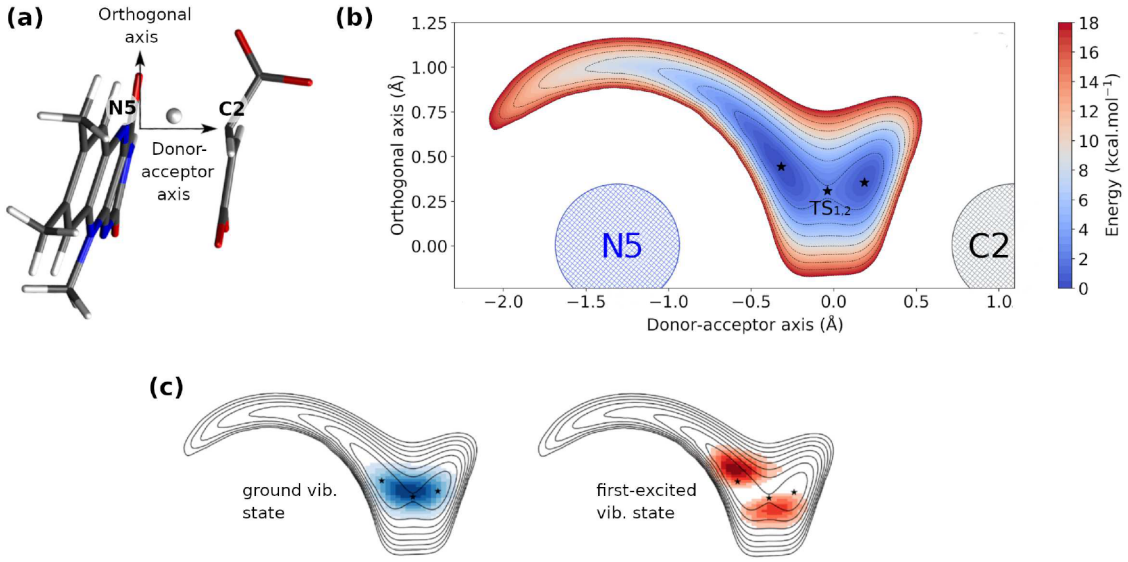

Figure 5. Vibrational analysis of the hydride transfer step **1** → **2**. (a) Flavin and fumarate geometries at the transition state, showing the donor−acceptor axis and the orthogonal axis. (b) Two-dimensional proton potential calculated at the $\mathbf{TS}_{1,2}$ geometry. (c) Amplitudes of the proton vibrational wave function.

$\Delta V_p^{\ddagger}$ (Table 1), suggesting the reaction is not only electronically adiabatic (as determined above) but also vibrationally adiabatic. That means electrons will respond instantaneously to the motion of the transferring proton, and the proton itself will respond instantaneously to the motion of the other nuclei.[70,71]

Table 1. Parameters Estimated for Nuclear Adiabaticity and Tunneling Effects for $\mathbf{TS}_{1,2}$ of the Hydride Transfer in 1 → 2 as Defined in the Main Text

parameter	value
Proton vibration adiabaticity	
$\Delta V_p^{\ddagger}$ (kcal·mol^{-1})	2.0
Δ_{vib} (kcal·mol^{-1})	2.7
Hydride tunneling	
$\nu^{\ddagger}$ (cm^{-1})	1268.5
κ	2.6

Nevertheless, it should be noted that the TS geometry is probably the most adiabatic region along the reaction coordinate as the active-site is preorganized to accommodate hydride transfer with the lowest possible energy barrier.[72] Therefore, the vibrationally adiabatic regime discussed here will only be valid at the TS and its shortest surroundings.

In the electronic and vibrational adiabatic regimes described for $\mathbf{TS}_{1,2}$, tunneling can still contribute to the rate of hydride transfer, as previously observed for other flavoproteins.[34,35] The simplest diagnostic for ground state tunneling in this regime is Wigner's first order correction[63−65] that calculates the transmission coefficient κ as a function of the modulus of the transition state imaginary frequency $\nu^{\ddagger}$ and the temperature T

$$\kappa \simeq 1 + \frac{1}{24}\left(\frac{hc\nu^{\ddagger}}{k_B T}\right)^2 \quad (1)$$

where h is Planck's constant, c is the speed of light, and k_B is the Boltzmann constant. Calculated parameters in Table 1 show that $\kappa = 2.6$ for $\mathbf{TS}_{1,2}$, consistent with small to moderate hydride tunneling.[63] This result is in accordance with the low deuterium kinetic isotope effects (KIEs) observed experimentally for this reaction.[27−29,68] Therefore, tunneling is present, but it is not critical for hydride transfer step in Fcc_3 enzyme kinetics.

A Large Electrostatic Dipole Stabilizes Hydride Transfer. Several strategies can be employed by enzymes to catalyze reactions.[73,74] We have shown in the previous section that Fcc_3 may protonate the fumarate C4 carboxylate by His504 in a relay type of general-acid catalysis (Figure 2b). We also discarded covalent catalysis in the form of intermediates covalently bound to the flavin ring because reactions that form adducts with FAD are too energetic (Figure 4).

Another common enzymatic strategy for TS stabilization is electrostatic catalysis.[73] This is employed by Fcc_3 to stabilize hydride transfer as suggested by the electrostatic potential of the large active-site cluster model shown in Figure 6. Hydride (H^-) is transferred in the axis perpendicular to the figure plane (the donor−acceptor axis in Figure 5) toward the positively charged region, i.e. the active site has its charge dipole preorganized to facilitate hydride transfer.

Another catalytic contribution often proposed to facilitate hydride transfer in FRD/SDH is a stereochemical constraint imposed by the active-site to twist fumarate carboxylate C1 into a less stable geometry[1,11,21,23] (Figure 1a). The optimized geometry found here for **1** has the C1−C2 bond twisted, in agreement with crystal structures of the enzyme complexed to fumarate.[11,20,21]

To check the stability and the hydride transfer barrier of planar fumarate, we performed constrained geometry optimizations to hold **1** and $\mathbf{TS}_{1,2}$ in a planar conformation. The corresponding optimized species are 6.0 and 16.0 kcal·mol^{-1} more energetic than their twisted (unconstrained) counterparts, respectively. The barrier for hydride transfer in a planar fumarate would be 33.0 kcal·mol^{-1} and is significantly higher than found for the twisted substrate (Figure 2). Thus, the FRD active site stabilizes a twisted fumarate (at C1−C2 bond) and lowers the barrier for hydride transfer, in comparison to a fully planar fumarate.

https://doi.org/10.1021/acs.jcim.3c00292
J. Chem. Inf. Model. XXXX, XXX, XXX−XXX

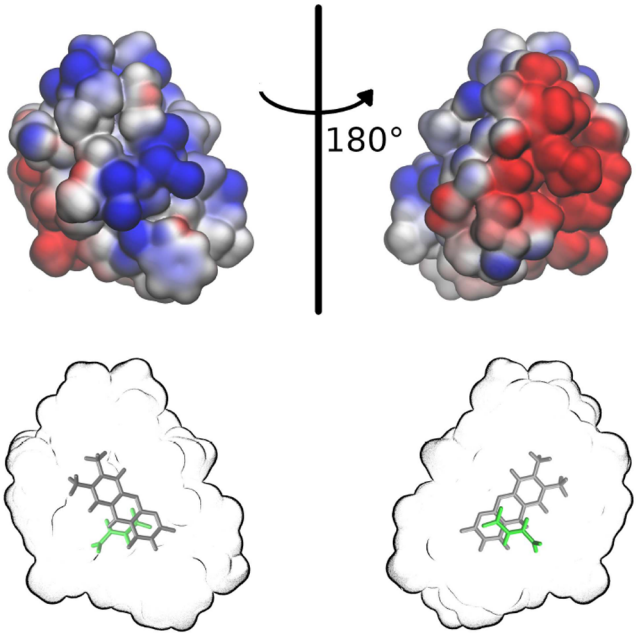

Figure 6. Electrostatic mapping of the active-site at the transition state $\mathbf{TS}_{1,2}$ geometry. The color scale ranges from blue to red for negatively charged regions ($-\delta$) to positively charged regions ($\delta+$), respectively. Hydride transfer takes place in the donor−acceptor axis normal to the plane of the figure. The lower panel shows the corresponding active site envelope with flavin in gray and fumarate in green.

Instead of the previously proposed substrate destabilization,[20] it is transition state stabilization that provides catalysis in FRDs. Fumarate twisting disrupts electron conjugation between C═C and C═O bonds and allows efficient hydride transfer. Note that the twisted bond does not affect the carbanion/enolate stabilization on the C3−C4 bond discussed above (Figure 3).

Thr377 coordinates fumarate and has been proposed to stabilize the twisted form (Figure 1a).[23] The role of Thr377 was probed here by changing this side-chain to alanine and rerunning geometry optimizations. In the computational mutant T377A, fumarate remained twisted indicating that the hydrogen-bond of the Thr377 side-chain to carboxylate C1 is not fundamental. Hydrogen-bonds with the His365 side-chain and the backbone of Glu378 are sufficient to stabilize the twisted conformation. Loss of activity observed on the experimental T377A mutation may be related to larger perturbations of the enzyme active-site such as increased hydration. We suggest mutation T377V to be tested experimentally, because the Val side-chain has a similar volume to Thr and potentially retains the ability to block entrance of water in the active site.

Regeneration of Catalytic Groups Drives Enzyme Turnover. In previous sections, only enzymatic steps involving fumarate reduction were discussed (**1**→ **3**). But, the complete Fcc_3 enzyme turnover also depends on product and substrate (un)binding, as well as regeneration of the catalytic FAD and Arg402 side-chain respectively from the oxidized and deprotonated (neutral) forms found in **3**.

The catalytic cycle proposed in Figure 7 suggests that succinate unbinds from state **3** to yield the oxidized unbound state **12** which can receive two-protons and two-electrons ($2\ H^+ + 2\ e^-$) and generate a reduced $FADH_2$ species **13**. We

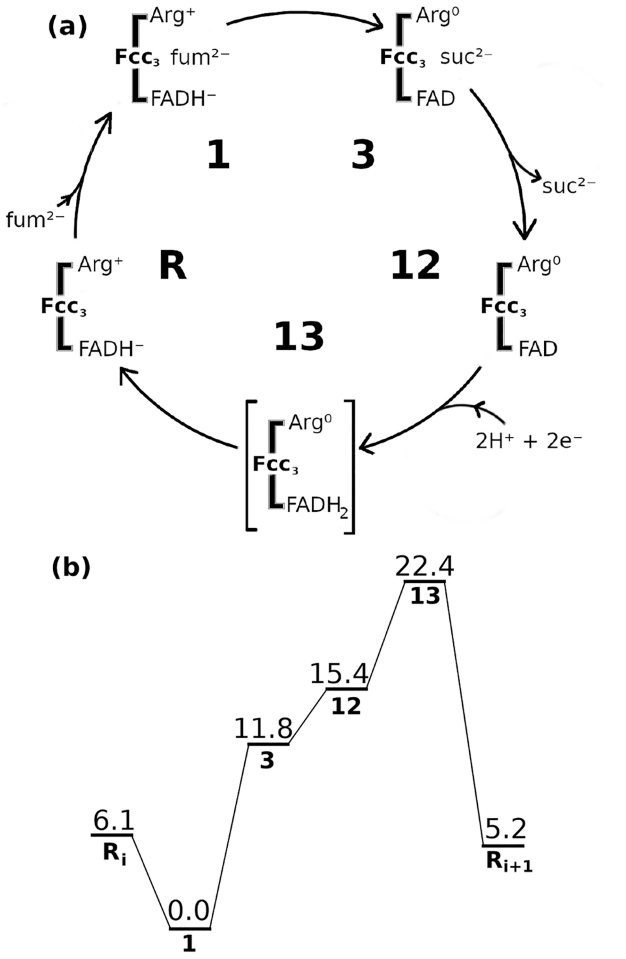

Figure 7. Complete enzymatic cycle (panel a) proposed for fumarate reduction and relative free energies (panel b) of cycle steps catalyzed by Fcc_3 FRD. States **1** and **3** are Michaelis complexes respectively with the fumarate (fum) reactant and succinate (suc) product, as shown in Figure 2. States **12** and **13** are the flavin oxidized and reduced unbound enzyme, respectively. $\mathbf{R}_i$ and $\mathbf{R}_{i+1}$ denote the resting enzymatic state before and after one cycle turnover. Free energies (in kcal·mol^{-1}) are shown over the bars, and species are identified by bold characters below the bars. Full lines are used to connect states because these are stable local minima and do not depict TS (as opposed to Figures 2 and 4).

propose this is an unstable species that readily decomposes to the reduced unbound state **R** with a proton transferred to Arg402. The resting state **R** may undergo another catalytic cycle after a fumarate substrate binds to generate the Michaelis complex **1**.

The proposed catalytic cycle is based on the energetic profile of Figure 7b. Free energies were obtained from a combination of calculated values for fumarate reduction (**1**→ **3** step, Figure 2) and for Arg402 regeneration (**13**→ **R**, see below) with experimental data. Binding free energies of fumarate (**R**→ **1**, K_M = 36 μM)[12] and succinate (**3**→ **12**, K_M = 2.2 mM)[12] were obtained from the experimental $K_M \approx K_D = \exp(-\Delta G/RT)$, where R is the gas constant. It has been shown for Fcc_3 that Michaelis constants K_M are similar to dissociation constants K_D.[14,75,76] The redox potential measured electrochemically for the flavin group in Fcc_3 ($E^{\circ\prime}$ = −0.152 V)[12] was used to estimate the free energy for step **12**→ **13**, as $\Delta G = -nFE^{\circ\prime}$, where n = 2 electrons, and F is the Faraday constant.

https://doi.org/10.1021/acs.jcim.3c00292
J. Chem. Inf. Model. XXXX, XXX, XXX−XXX

Experiments were conducted under similar conditions and biochemical states of T = 298 K and pH = 7.0, except for the succinate K_M obtained at pH = 8.0. For calculated steps (**1**→ **3** and **13**→ **R**), standard state corrections are not necessary as the total molecular composition does not change.

Reduction of FAD involves electron transfer from heme groups in Fcc_3 or from iron−sulfur clusters in other FRD/SDH enzymes. Both cofactors are only capable of one-electron reductions, producing radical (flavosemiquinone) intermediates, often coupled to proton transfers.[77,78] Modeling such reduction processes in detail is challenging and out of the scope of the present study.

Here, we assume that a biprotonated reduced flavin ($FADH_2$) with neutral Arg402 side-chain state (**13**) is transiently formed and calculate the free energy for its conversion to the regenerated and "ready-to-react" resting state **R**, with monoprotonated reduced flavin ($FADH^-$) and protonated Arg402 side-chain (Figure 7a). Applying the same large active-site cluster and model chemistry used for fumarate reduction, reaction **13**→ **R** has a calculated free energy ΔG = −17.2 kcal·mol^{-1}. It is notable that a similar value (−18.0 kcal·mol^{-1}) is obtained for the same process if succinate remains bound at the active site model. Thus, the energy difference between **12** and the transient species **13** is independent of whether succinate is bound or not to the active site, and an alternative enzymatic cycle with succinate unbinding *after* FAD reduction cannot be ruled out.

Summing over free energies estimated for each step in the proposed catalytic cycle results in −0.9 kcal·mol^{-1} (Figure 7). It corresponds to the free energy released after one complete enzyme turnover ($\mathbf{R}_i$→ $\mathbf{R}_{i+1}$) and is the same free energy value obtained from the measured fumarate → succinate redox potential in enzyme-free water solution ($E^{\circ\prime}$ = +0.03 V).[79] This excellent thermodynamic agreement supports the presence of transient step **13** and the proposed cycle. Otherwise, assignment of the measured flavin redox potential in Fcc_3 ($E^{\circ\prime}$ = −0.152 V)[12] to a direct conversion **12**→ **R** would result in a disagreement of more than 15 kcal·mol^{-1} between the enzymatic cycle thermodynamics estimated here and the experimental redox free energy for the uncatalyzed reaction in water.

It has been proposed that the neutral side-chain of Arg402 is reprotonated by an excess proton from the solvent via a Grotthuss mechanism.[18,23] We computed the free energies associated with this process by turning one of the structural waters near the solvent boundary and Glu378 in the large active-site model (Figure 1b) of state **3** into a hydronium, without altering the FAD redox state, and found the overall reaction is very exergonic (Figure S1).

Thus, regeneration of Arg402, either coupled to FAD reduction and decomposition of the transient species **13** (Figure 7b) or directly from the solvent and uncoupled from FAD redox (Figure S1), provides the driving force to complete the Fcc_3 catalytic cycle.

Succinate oxidation would proceed by reversing the catalytic cycle (counterclockwise in Figure 7a). But this process will have a high activation energy (**R**→ **13**), corroborating experimental observations that Fcc_3 is unable to catalyze the reverse transformation.[1,12] Other FRD/SDH enzymes with a covalently bound flavin may stabilize states equivalent to **13** and hence catalyze succinate oxidation, as supported by the significantly higher redox potential ($\Delta E^{\circ\prime} \approx$ 0.1 V) measured in such enzymes.[1,36]

The experimental turnover rate k_{cat} = 370 s^{-1} for fumarate reduction corresponds to an effective barrier of 13.9 kcal·mol^{-1},[14] using canonical transition state theory. Considering the activation energy of 23 ± 4 kcal·mol^{-1} calculated here for $\mathbf{TS}_{1,2}$ and $\mathbf{TS}_{2,3}$ or formation of transient state **13** with a free energy of 22 ± 4 kcal·mol^{-1} as rate-determining steps suggests an offset error of at least 4−5 kcal·mol^{-1} for the calculated overall turnover barrier. This error may be attributed to a lack long-range electrostatic interactions beyond the cluster model and possible hydride and proton ("deep") tunneling before reaching the TS, both of which were not included in the present calculations.

CONCLUSIONS

Catalysis of fumarate reduction to succinate by the FRD enzyme Fcc_3 was dissected here using calibrated and highly accurate electronic structure calculations. Reaction mechanisms involving adducts or radical (and carbocation) intermediates were unequivocally discarded, confirming the current experimental view that fumarate reduction occurs in two steps via a carbanion intermediate. This intermediate, however, is best described as an enolate electromer. In the most likely mechanism found here, hydride transfer from $FADH^-$ and proton transfer from Arg402 proceed stepwisely in this order. Both processes have equivalent energy barriers and contribute to the effective activation energy. Protonation of one fumarate carboxylate (C4) in a relay mechanism prior to hydride transfer cannot be discarded but appears to be unnecessary for catalysis.

Sources of the catalytic power in FRD/SDH were probed here. The electrostatic potential of the active site with a large charge dipole gives directionality and stabilizes hydride transfer toward fumarate. The twisted conformation of fumarate is also fundamental for catalysis by providing a high stabilization energy for the transition state of hydride addition. Substrate destabilization and its hydrogen-bond to Thr377 were shown to be less relevant for catalysis. Hydride transfer was shown to be adiabatic and with low tunneling contribution near the transition state. But, more research is required to rule out tunneling ("deep" or corner-cutting) in other parts of the potential energy surface.

Enzyme regeneration provides the thermodynamic driving force for enzyme turnover. Reprotonation of the catalytic Arg402, either coupled to FAD reduction and decomposition of the proposed transient state (**13**) or directly from the solvent, is highly exergonic. These findings can be extrapolated to other fumarate reductases and to succinate dehydrogenases. But the effect of a covalently bound FAD, as found in membrane-associated enzymes, has yet to be addressed in future studies.

ASSOCIATED CONTENT

Data Availability Statement

Data underlying this study are openly available online (Zenodo) at https://doi.org/10.5281/zenodo.7886942.

Supporting Information

The Supporting Information is available free of charge at https://pubs.acs.org/doi/10.1021/acs.jcim.3c00292.

Detailed calibration of the computational methods and models employed here, a table with energy comparisons to various DFT functionals, a figure with the free energy

https://doi.org/10.1021/acs.jcim.3c00292
J. Chem. Inf. Model. XXXX, XXX, XXX−XXX

of Arg402 regeneration, and a figure with wave function analysis (PDF)

Four videos showing the computed reaction mechanisms and free energy profiles (ZIP)

AUTHOR INFORMATION

Corresponding Author

Guilherme M. Arantes − *Department of Biochemistry, Instituto de Química, Universidade de São Paulo, 05508-900 São Paulo, São Paulo, Brazil;* orcid.org/0000-0001-5356-7703; Email: garantes@iq.usp.br

Author

Felipe Curtolo − *Department of Biochemistry, Instituto de Química, Universidade de São Paulo, 05508-900 São Paulo, São Paulo, Brazil;* orcid.org/0000-0002-4459-0968

Complete contact information is available at: https://pubs.acs.org/10.1021/acs.jcim.3c00292

Notes

The authors declare no competing financial interest.

ACKNOWLEDGMENTS

Funding from Fundação de Amparo à Pesquisa do Estado de São Paulo (FAPESP, scholarships 2016/23525-0 and 2017/26109-0 to F.C., and grants 2019/21856-7 and 2023/00934-5 to G.M.A.) is gratefully acknowledged. This work is dedicated to the memory of Eden Douglas Arantes - father, doctor, and inspiration.

REFERENCES

(1) Iverson, T. Catalytic mechanisms of complex II enzymes: A structural perspective. *Biochim. Biophys. Acta* **2013**, *1827*, 648−657.

(2) Pealing, S. L.; Black, A. C.; Manson, F. D. C.; Ward, F. B.; Chapman, S. K.; Reid, G. A. Sequence of the Gene Encoding Flavocytochrome *c* from *Shewanella putrefaciens*: A Tetraheme Flavoenzyme That Is a Soluble Fumarate Reductase Related to the Membrane-Bound Enzymes from Other Bacteria. *Biochemistry* **1992**, *31*, 12132−12140.

(3) Kim, S.; Kim, C. M.; Son, Y.-J.; Choi, J. Y.; Siegenthaler, R. K.; Lee, Y.; Jang, T.-H.; Song, J.; Kang, H.; Kaiser, C. A.; Park, H. H. Molecular basis of maintaining an oxidizing environment under anaerobiosis by soluble fumarate reductase. *Nat. Commun.* **2018**, *9*, 4867.

(4) Sakai, C.; Tomitsuka, E.; Esumi, H.; Harada, S.; Kita, K. Mitochondrial fumarate reductase as a target of chemotherapy: From parasites to cancer cells. *Biochim. Biophys. Acta Gen. Subj.* **2012**, *1820*, 643−651.

(5) Soares, R. O. S.; Losada, D. M.; Jordani, M. C.; Évora, P.; Castro-e-Silva, O. Ischemia/Reperfusion Injury Revisited: An Overview of the Latest Pharmacological Strategies. *Int. J. Mol. Sci.* **2019**, *20*, 5034.

(6) Wardrope, C.; Mowat, C. G.; Walkinshaw, M. D.; Reid, G. A.; Chapman, S. K. Fumarate reductase: Structural and mechanistic insights from the catalytic reduction of 2-methylfumarate. *FEBS Lett.* **2006**, *580*, 1677−1680.

(7) Karavaeva, V.; Sousa, F. L. Modular structure of complex II: An evolutionary perspective. *Biochim. Biophys. Acta Bioenerg.* **2023**, *1864*, 148916.

(8) Maklashina, E. Structural Insight into Evolution of the Quinone Binding Site in Complex II. *Biochemistry Moscow* **2022**, *87*, 752−761.

(9) Reid, G. A.; Gordon, E. H. J.; Hill, A. E.; Doherty, M.; Turner, K.; Holt, R.; Chapman, S. K. Structure and function of flavocytochrome c_3, the soluble fumarate reductase from Shewanella NCIMB400. *Biochem. Soc. Trans.* **1998**, *26*, 418−421.

(10) Williams, C. C.; Jan, C. H.; Weissman, J. S. Targeting and plasticity of mitochondrial proteins revealed by proximity-specific ribosome profiling. *Science* **2014**, *346*, 748−751.

(11) Taylor, P.; Pealing, S. L.; Reid, G. A.; Chapman, S. K.; Walkinshaw, M. D. Structural and mechanistic mapping of a unique fumarate reductase. *Nat. Struct. Biol.* **1999**, *6*, 1108−1112.

(12) Turner, K. L.; Doherty, M. K.; Heering, H. A.; Armstrong, F. A.; Reid, G. A.; Chapman, S. K. Redox Properties of Flavocytochrome c_3 from *Shewanella frigidimarina NCIMB400*. *Biochemistry* **1999**, *38*, 3302−3309.

(13) Bamford, V.; Dobbin, P. S.; Richardson, D. J.; Hemmings, A. M. Open conformation of a flavocytochrome c_3 fumarate reductase. *Nat. Struct. Biol.* **1999**, *6*, 1104−1107.

(14) Doherty, M. K.; Pealing, S. L.; Miles, C. S.; Moysey, R.; Taylor, P.; Walkinshaw, M. D.; Reid, G. A.; Chapman, S. K. Identification of the Active Site Acid/Base Catalyst in a Bacterial Fumarate Reductase: A Kinetic and Crystallographic Study. *Biochemistry* **2000**, *39*, 10695−10701.

(15) Mowat, C. G.; Moysey, R.; Miles, C. S.; Leys, D.; Doherty, M. K.; Taylor, P.; Walkinshaw, M. D.; Reid, G. A.; Chapman, S. K. Kinetic and Crystallographic Analysis of the Key Active Site Acid/Base Arginine in a Soluble Fumarate Reductase. *Biochemistry* **2001**, *40*, 12292−12298.

(16) Pankhurst, K. L.; Mowat, C. G.; Miles, C. S.; Leys, D.; Walkinshaw, M. D.; Reid, G. A.; Chapman, S. K. Role of His505 in the Soluble Fumarate Reductase from *Shewanella frigidimarina*. *Biochemistry* **2002**, *41*, 8551−8556.

(17) Rothery, E. L.; Mowat, C. G.; Miles, C. S.; Mott, S.; Walkinshaw, M. D.; Reid, G. A.; Chapman, S. K. Probing Domain Mobility in a Flavocytochrome. *Biochemistry* **2004**, *43*, 4983−4989.

(18) Pankhurst, K. L.; Mowat, C. G.; Rothery, E. L.; Hudson, J. M.; Jones, A. K.; Miles, C. S.; Walkinshaw, M. D.; Armstrong, F. A.; Reid, G. A.; Chapman, S. K. A Proton Delivery Pathway in the Soluble Fumarate Reductase from *Shewanella frigidimarina*. *J. Biol. Chem.* **2006**, *281*, 20589−20597.

(19) Sun, F.; Huo, X.; Zhai, Y.; Wang, A.; Xu, J.; Su, D.; Bartlam, M.; Rao, Z. Crystal Structure of Mitochondrial Respiratory Membrane Protein Complex II. *Cell* **2005**, *121*, 1043−1057.

(20) Lancaster, C. R. D.; Kröger, A.; Auer, M.; Michel, H. Structure of fumarate reductase from *Wolinella succinogenes* at 2.2 Å resolution. *Nature* **1999**, *402*, 377−385.

(21) Tomasiak, T. M.; Archuleta, T. L.; Andréll, J.; Luna-Chávez, C.; Davis, T. A.; Sarwar, M.; Ham, A. J.; McDonald, W. H.; Yankovskaya, V.; Stern, H. A.; Johnston, J. N.; Maklashina, E.; Cecchini, G.; Iverson, T. M. Geometric Restraint Drives On- and Off-pathway Catalysis by the *Escherichia coli* Menaquinol:Fumarate Reductase. *J. Biol. Chem.* **2011**, *286*, 3047−3056.

(22) Schröder, I.; Gunsalus, R. P.; Ackrell, B. A. C.; Cochran, B.; Cecchini, G. Identification of Active Site Residues of *Escherichia coli* Fumarate Reductase by Site-directed Mutagenesis. *J. Biol. Chem.* **1991**, *266*, 13572−13579.

(23) Tomasiak, T. M.; Maklashina, E.; Cecchini, G.; Iverson, T. M. A Threonine on the Active Site Loop Controls Transition State Formation in *Escherichia coli* Respiratory Complex II. *J. Biol. Chem.* **2008**, *283*, 15460−15468.

(24) Blaut, M.; Whittaker, K.; Valdovinos, A.; Ackrell, B. A. C.; Gunsalus, R. P.; Cecchini, G. Fumarate Reductase Mutants of *Escherichia coli* That Lack Covalently Bound Flavin. *J. Biol. Chem.* **1989**, *264*, 13599−13604.

(25) Tedeschi, G.; Ronchi, S.; Simonic, T.; Treu, C.; Mattevi, A.; Negri, A. Probing the Active Site of $_L$-Aspartate Oxidase by Site-Directed Mutagenesis: Role of Basic Residues in Fumarate Reduction. *Biochemistry* **2001**, *40*, 4738−4744.

(26) Curtolo, F.; Arantes, G. M. Mechanisms for Flavin-Mediated Oxidation: Hydride or Hydrogen-Atom Transfer? *J. Chem. Inf. Model.* **2020**, *60*, 6282−6287.

(27) Vitale, L.; Rittenberg, D. The Rates of Oxidation of Some Deuterio Isomers of Succinate by Succinic Dehydrogenase. *Biochemistry* **1967**, *6*, 690−699.

https://doi.org/10.1021/acs.jcim.3c00292
J. Chem. Inf. Model. XXXX, XXX, XXX−XXX

(28) Hollocher, T. C.; You, K.-s.; Conjalka, M. Rate-Determining Steps in the Oxidation of Succinate Catalyzed by Succinic Dehydrogenase. *J. Am. Chem. Soc.* **1970**, *92*, 1032−1035.
(29) Kaczorowski, G. J.; Cheung, Y.-F.; Walsh, C. Substrate Kinetic Isotope Effects in Dehydrogenase Coupled Active Transport in Membrane Vesicles of *Escherichia coli*. *Biochemistry* **1977**, *16*, 2619−2628.
(30) Huang, L.-S.; Shen, J. T.; Wang, A. C.; Berry, E. A. Crystallographic studies of the binding of ligands to the dicarboxylate site of Complex II, and the identity of the ligand in the "oxaloacetate-inhibited" state. *Biochim. Biophys. Acta* **2006**, *1757*, 1073−1083.
(31) Lucas, M. F.; Ramos, M. J. Mechanism of a Soluble Fumarate Reductase from Shewanella frigidimarina: A Theoretical Study. *J. Phys. Chem. B* **2006**, *110*, 10550−10556.
(32) Venkataram, U. V.; Bruice, T. C. On the Mechanism of Flavin-Catalyzed Dehydrogenation α,β to an Acyl Function. The Mechanism of 1,5-Dihydroflavin Reduction of Maleimides. *J. Am. Chem. Soc.* **1984**, *106*, 5703−5709.
(33) Dai, Y.; Kizjakina, K.; Campbell, A. C.; Korasick, D. A.; Tanner, J. J.; Sobrado, P. Flavin-N5 Covalent Intermediate in a Nonredox Dehalogenation Reaction Catalyzed by an Atypical Flavoenzyme. *ChemBioChem.* **2018**, *19*, 53−57.
(34) Pang, J.; Hay, S.; Scrutton, N. S.; Sutcliffe, M. J. Deep Tunneling Dominates the Biologically Important Hydride Transfer Reaction from NADH to FMN in Morphinone Reductase. *J. Am. Chem. Soc.* **2008**, *130*, 7092−7097.
(35) Delgado, M.; Görlich, S.; Longbotham, J. E.; Scrutton, N. S.; Hay, S.; Moliner, V.; Tuñón, I. Convergence of Theory and Experiment on the Role of Preorganization, Quantum Tunneling, and Enzyme Motions into Flavoenzyme-Catalyzed Hydride Transfer. *ACS Catal.* **2017**, *7*, 3190−3198.
(36) Léger, C.; Heffron, K.; Pershad, H. R.; Maklashina, E.; Luna-Chavez, C.; Cecchini, G.; Ackrell, B. A. C.; Armstrong, F. A. Enzyme Electrokinetics: Energetics of Succinate Oxidation by Fumarate Reductase and Succinate Dehydrogenase. *Biochemistry* **2001**, *40*, 11234−11245.
(37) Cheng, V. W. T.; Piragasam, R. S.; Rothery, R. A.; Maklashina, E.; Cecchini, G.; Weiner, J. H. Redox State of Flavin Adenine Dinucleotide Drives Substrate Binding and Product Release in *Escherichia coli* Succinate Dehydrogenase. *Biochemistry* **2015**, *54*, 1043−1052.
(38) Prejanò, M.; Marino, T.; Russo, N. QM Cluster or QM/MM in Computational Enzymology: The Test Case of LigW-Decarboxylase. *Front. Chem.* **2018**, *6*, 249.
(39) Siegbahn, P. E.; Himo, F. The quantum chemical cluster approach for modeling enzyme reactions. *WIREs Comput. Mol. Sci.* **2011**, *1*, 323−336.
(40) Curtolo, F.; Arantes, G. M. Molecular properties and tautomeric equilibria of isolated flavins. *J. Comput. Chem.* **2022**, *43*, 1561−1572.
(41) Harms, M. J.; Schlessman, J. L.; Sue, G. R.; García-Moreno E, B. Arginine residues at internal positions in a protein are always charged. *Proc. Natl. Acad. Sci. U.S.A.* **2011**, *108*, 18954−18959.
(42) Grimme, S.; Antony, J.; Ehrlich, S.; Krieg, H. A Consistent and Accurate ab initio Parametrization of Density Functional Dispersion Correction (DFT-D) for the 94 Elements H-Pu. *J. Chem. Phys.* **2010**, *132*, 154104.
(43) Lin, Y. S.; Li, G. D.; Mao, S. P.; Chai, J. D. Long-Range Corrected Hybrid Density Functionals with Improved Dispersion Corrections. *J. Chem. Theory Comput.* **2013**, *9*, 263−722.
(44) Weigend, F.; Ahlrichs, R. Balanced Basis Sets of Split Valence, Triple Zeta Valence and Quadruple Zeta Valence Quality for H to Rn: Design and Assessment of Accuracy. *Phys. Chem. Chem. Phys.* **2005**, *7*, 3297−3305.
(45) Spicher, S.; Grimme, S. Single-Point Hessian Calculations for Improved Vibrational Frequencies and Rigid-Rotor-Harmonic-Oscillator Thermodynamics. *J. Chem. Theory Comput.* **2021**, *17*, 1701−1714.
(46) Angeli, C.; Cimiraglia, R.; Evangelisti, S.; Leininger, T.; Malrieu, J.-P. Introduction of *n*-electron valence states for multi-reference perturbation theory. *J. Chem. Phys.* **2001**, *114*, 10252−10264.
(47) Angeli, C.; Cimiraglia, R.; Malrieu, J.-P. n-electron valence state perturbation theory: A spinless formulation and an efficient implementation of the strongly contracted and of the partially contracted variants. *J. Chem. Phys.* **2002**, *117*, 9138−9153.
(48) Neese, F. The ORCA program system. *WIREs Comput. Mol. Sci.* **2012**, *2*, 73−78.
(49) Neese, F. Software Update: The ORCA Program System. *Version 4.0. WIREs Rev. Comput. Mol. Sci.* **2018**, *8*, e1327.
(50) Barone, V.; Cossi, M. Quantum Calculation of Molecular Energies and Energy Gradients in Solution by a Conductor Solvent Model. *J. Phys. Chem. A* **1998**, *102*, 1995−2001.
(51) Nunes-Alves, A.; Arantes, G. M. Ligand-receptor affinities computed by an adapted linear interaction model for continuum electrostatics and by protein conformational averaging. *J. Chem. Inf. Model.* **2014**, *54*, 2309−2319.
(52) Grimme, S.; Brandenburg, J. G.; Bannwarth, C.; Hansen, A. Consistent structures and interactions by density functional theory with small atomic orbital basis sets. *J. Chem. Phys.* **2015**, *143*, 054107.
(53) Grimme, S.; Ehrlich, S.; Goerigk, L. Effect of the damping function in dispersion corrected density functional theory. *J. Comput. Chem.* **2011**, *32*, 1456−1465.
(54) Kruse, H.; Grimme, S. A geometrical correction for the inter- and intra-molecular basis set superposition error in Hartree-Fock and density functional theory calculations for large systems. *J. Chem. Phys.* **2012**, *136*, 154101.
(55) Ishida, K.; Morokuma, K.; Komornicki, A. The intrinsic reaction coordinate. An *ab initio* calculation for HNC→ HCN and H^-+CH4→CH4+H^-. *J. Chem. Phys.* **1977**, *66*, 2153−2156.
(56) Curtolo, F.; Arantes, G. M. Dataset: Dissecting reaction mechanisms and catalytic contributions in flavoprotein fumarate reductases. *Zenodo* 2023, https://doi.org/10.5281/zenodo.7886942 (accessed 2023-05-17).
(57) Grimme, S. Supramolecular Binding Thermodynamics by Dispersion-Corrected Density Functional Theory. *Chem.—Eur. J.* **2012**, *18*, 9955−9964.
(58) Bannwarth, C.; Ehlert, S.; Grimme, S. GFN2-xTB−An Accurate and Broadly Parametrized Self-Consistent Tight-Binding Quantum Chemical Method with Multipole Electrostatics and Density-Dependent Dispersion Contributions. *J. Chem. Theory Comput.* **2019**, *15*, 1652−1671.
(59) Bannwarth, C.; Caldeweyher, E.; Ehlert, S.; Hansen, A.; Pracht, P.; Seibert, J.; Spicher, S.; Grimme, S. Extended tight-binding quantum chemistry methods. *WIREs Comput. Mol. Sci.* **2021**, *11*, e1493.
(60) Marston, C. C.; Balint-Kurti, G. G. The Fourier grid Hamiltonian method for bound state eigenvalues and eigenfunctions. *J. Chem. Phys.* **1989**, *91*, 3571−3576.
(61) Soudackov, A.; Hammes-Schiffer, S. Derivation of Rate Expressions for Nonadiabatic Proton-Coupled Electron Transfer Reactions in Solution. *J. Chem. Phys.* **2000**, *113*, 2385−2396.
(62) Soudackov, A. V.; Hammes-Schiffer, S. *fgh_casci_3d*. http://webpcet.chem.yale.edu/downloads.html (accessed 2022-08-31).
(63) Nandi, A.; Molpeceres, G.; Gupta, P. K.; Major, D. T.; Kästner, J.; Martin, J. M.; Kozuch, S. Quantum Tunneling in Computational Catalysis and Kinetics: Is it Really Important? In *Reference Module in Chemistry, Molecular Sciences and Chemical Engineering*; Elsevier: 2022.
(64) Bell, R. P. The application of tunnel corrections in chemical kinetics. In *The Tunnel Effect in Chemistry*; Springer: Boston, 1980; Chapter 3, pp 51−76.
(65) Wigner, E. P. Über das Überschreiten von Potentialschwellen bei chemischen Reaktionen. *Z. Phys. Chem.* **1932**, *19B*, 203−216.
(66) Darcy, J. W.; Koronkiewicz, B.; Parada, G. A.; Mayer, J. M. A Continuum of Proton-Coupled Electron Transfer Reactivity. *Acc. Chem. Res.* **2018**, *51*, 2391−2399.

https://doi.org/10.1021/acs.jcim.3c00292
J. Chem. Inf. Model. XXXX, XXX, XXX−XXX

(67) Kozuch, S.; Shaik, S. How to Conceptualize Catalytic Cycles? The Energetic Span Model. *Acc. Chem. Res.* **2011**, *44*, 101−110.
(68) Hirst, J.; Ackrell, B. A. C.; Armstrong, F. A. Global Observation of Hydrogen/Deuterium Isotope Effects on Bidirectional Catalytic Electron Transport in an Enzyme: Direct Measurement by Protein-Film Voltammetry. *J. Am. Chem. Soc.* **1997**, *119*, 7434−7439.
(69) Hammes-Schiffer, S. Comparison of Hydride, Hydrogen Atom, and Proton-Coupled Electron Transfer Reactions. *ChemPhysChem* **2002**, *3*, 33−42.
(70) Skone, J. H.; Soudackov, A. V.; Hammes-Schiffer, S. Calculation of Vibronic Couplings for Phenoxyl/Phenol and Benzyl/Toluene Self-Exchange Reactions: Implications for Proton-Coupled Electron Transfer Mechanisms. *J. Am. Chem. Soc.* **2006**, *128*, 16655−16663.
(71) Hammes-Schiffer, S. Proton-Coupled Electron Transfer: Classification Scheme and Guide to Theoretical Methods. *Energy Environ. Sci.* **2012**, *5*, 7696−7703.
(72) Hammes-Schiffer, S.; Stuchebrukhov, A. A. Theory of Coupled Electron and Proton Transfer Reactions. *Chem. Rev.* **2010**, *110*, 6939−6960.
(73) Warshel, A.; Sharma, P. K.; Kato, M.; Xiang, Y.; Liu, H.; Olsson, M. H. M. Electrostatic Basis for Enzyme Catalysis. *Chem. Rev.* **2006**, *106*, 3210−3235.
(74) Arantes, G. M. A computational perspective on enzymatic catalysis. *Quim. Nova* **2008**, *31*, 377−383.
(75) Morris, C. J.; Black, A. C.; Pealing, S. L.; Manson, F. D. C.; Chapman, S. K.; Reid, G. A.; Gibson, D. M.; Ward, F. B. Purification and properties of a novel cytochrome: flavocytochrome c from *Shewanella putrefaciens*. *Biochem. J.* **1994**, *302*, 587−593.
(76) Pealing, S. L.; Cheesman, M. R.; Reid, G. A.; Thomson, A. J.; Ward, F. B.; Chapman, S. K. Spectroscopic and Kinetic Studies of the Tetraheme Flavocytochrome c From Shewanella putrefaciens NCIMB400. *Biochemistry* **1995**, *34*, 6153−6158.
(77) Warren, J. J.; Mayer, J. M. Proton-Coupled Electron Transfer Reactions at a Heme-Propionate in an Iron-Protoporphyrin-IX Model Compound. *J. Am. Chem. Soc.* **2011**, *133*, 8544−8551.
(78) Camilo, S. R. G.; Curtolo, F.; Galassi, V. V.; Arantes, G. M. Tunneling and Nonadiabatic Effects on a Proton-Coupled Electron Transfer Model for the Q_o Site in Cytochrome bc_1. *J. Chem. Inf. Model.* **2021**, *61*, 1840−1849.
(79) Loach, P. A. Oxidation-Reduction Potentials, Absorbance Bands, and Molar Absorbance of Compounds Used in Biochemical Studies. In *Handbook of Biochemistry and Molecular Biology*, 5th ed.; Lundblad, R. L., Macdonald, F. M., Eds.; CRC Press: Boca Raton, 2018; Chapter 71, pp 576−582.

https://doi.org/10.1021/acs.jcim.3c00292
J. Chem. Inf. Model. XXXX, XXX, XXX−XXX